COMPARISON OF AEROELASTIC SOLUTIONS ON THE HIRENASD MODEL

A.-S. Sens,
ONERA, the French Aerospace Lab, B.P. 72, 29 avenue de la Division Leclerc, 92322 Châtillon Cedex, France
Anne-sophie.Sens@onera.fr

D.E. Raveh
Faculty of Aerospace Engineering, Technion – IIT, Haifa, Israel
Daniella@technion.ac.il

Keywords: Aeroelasticity, Navier-Stokes computation, static coupling, harmonic forced motion.

Abstract.
This paper presents numerical computations that were performed for the High Reynolds Number Aero-Structural Dynamics (HIRENASD) configuration in the context of the first aeroelastic prediction Workshop (AePW). Two partners involved in this workshop used their computational software to obtain the results: the EZNSS code of the Israeli CFD Center and the aeroelastic elsA/Ael software developed by Onera. The two softwares are structured. The analysis results include aerodynamic coefficients and surface pressures obtained for static aeroelastic equilibrium, and unsteady results induced by a forced motion at the 2nd Bending mode. Results are shown using different grid sizes, turbulence model and temporal convergence for some unsteady cases. Computational results are presented together with the corresponding experimental data.

1 INTRODUCTION

The main objective of the 1st NASA Langley Aeroelastic Prediction Workshop (AePW) was to assess the state-of-the-art high fidelity aeroelastic simulation tools for the prediction of both static and dynamic aeroelastic phenomena on relevant geometries. This Workshop took place in conjunction with the AIAA Structures, Structural Dynamics, and Materials Conference, on April 21-22, 2012, in Honolulu, Hawaï. Time accurate aerodynamic and aeroelastic computations using a large variety of codes and grids were performed by 17 participants from 10 nations. A selected set of unsteady aerodynamics and aeroelastic problems for which experimental data are available, has been investigated. A description of the workshop formation and execution can be found in [1].

The High Reynolds Number Aero-Structural Dynamics (HIRENASD) model was one of the three configurations selected for the numerical aeroelastic investigations. The HIRENASD wind tunnel experiment was conducted in the cryogenic European Wind Tunnel (ETW) by Aachen University with funding by the German Research Foundation, in 2006 [2,3,4]. The main purpose of this experiment was to provide a better aero-structural dynamics understanding and knowledge in the transonic regime up to flight Reynolds numbers, and also to get experimental data in a wide range of Reynolds numbers and aerodynamic loads for current and future aerodynamic and aeroelastic research.

This paper focuses on the numerical results of two partners involved in the AePW workshop: Onera (France) and the Technion, Israel Institute of Technology. Two structured grid softwares have been used: the in-house EZNSS code of Technion University and the elsA software developed by Onera.

The elsA code is a multi-block structured solver, based on an object-oriented approach [5,6] that allows to perform steady and unsteady aerodynamic simulations for viscous and non viscous flows. It handles RANS and URANS equations with a large set of turbulence models. This solver has been extended for aeroelastic simulations. The extended aeroelastic elsA/Ael version gives access to static and dynamic coupling simulations using different levels of structural modeling (reduced flexibility matrix, modal approach), and also to forced motion simulations [7,8]. Grid deformation techniques are also implemented in order to take into account the structural deformations and motion of geometries.

The EZNSS code is a multi-zone Euler/ Navier-Stokes flow solver which is capable of simulating complex, time-accurate flows about dynamically deforming geometries. This includes relative motion between surfaces as well as deformations induced by flexibility. The code contains a number of implicit algorithms and a number of turbulence models. The code handles complex geometries using patched grids or the Chimera overset grid topology. ENZSS solves the static or dynamic aeroelastic equation of motion in modal coordinates.

Static coupling as well as dynamic response simulations to a prescribed excitation have been carried out by the partners and compared with the available experimental data. A subsonic flow case and two transonic flow conditions with different Reynolds numbers and aerodynamic loads have been investigated by the different contributors.

Additional investigations have also been performed in order to study the effect of turbulence modeling (k-omega versus Spalart-Allmaras), and also the influence of some numerical parameters on the unsteady results (time-step size, number of internal iterations at each physical time-step).

2 HIRENASD WIND TUNNEL CONFIGURATION

The HIRENASD model was one of the configurations chosen for analysis in the AePW into aeroelastic analysis of systems with weak coupling between the fluid and the structure. The model (figure 1) has a 34˚ swept wing with a BAC3-11 supercritical airfoil profile, a span from root to tip of approximately 1.30 meters, and a mean aerodynamic chord of 0.3445 meters. In the first wing section from the root, the profile thickness was modified such that it varies linearly from 15% at the root to 11% at the transition to second section. In both outer sections the relative thickness remains constant at 11%. It is a semi-span model, ceiling mounted through a non-contracting fuselage fairing to a turntable, balance and excitation system. To enable dynamic aeroelastic experiments forces coupled acting in spanwise direction can be applied to the wing root plane by a vibrational excitation mechanism that is housed inside the wing clamped device. The latter is connected to the balance by a cylindrical shell. Extensive measurements were acquired during test. Instrumentation included 259 unsteady pressures transducers distributed along the upper and lower surface at seven span sections. In addition balance measurements and accelerations were obtained.

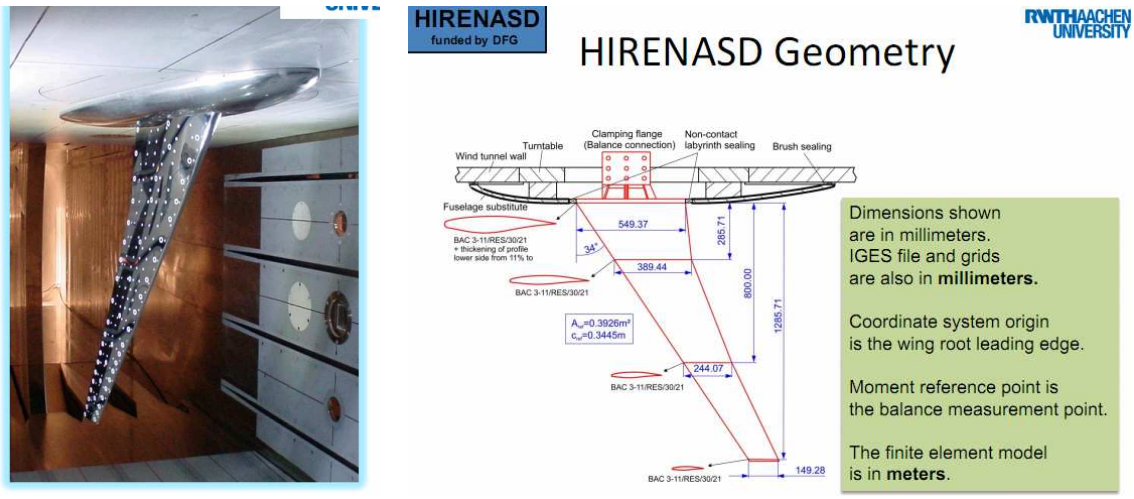

Figure 1: HIRENASD experimental set up at ETW and wing model dimension

For the Workshop, steady and time dependent analysis at two different Mach numbers, two different incidences and two different Reynolds number were suggested. All forced oscillation data used in AePW involved excitation near the wing's second bending mode frequency. These experimental data from HIRENASD experiments correspond to:

- ETW 129&155 case: Mach number = 0.7, Re = 7 $*10^6$, α=1.5°;
- ETW 132&159 case: Mach number = 0.8, Re = 7 $*10^6$, α=1.5°;
- ETW 250&271 case: Mach number = 0.8, Re = 23.5 $*10^6$, α= -1.34°.

All tests were conducted with nitrogen (γ=1.4) as test medium.

One of the challenges in using HIRENASD was generating a structural dynamic model that was well understood by the Workshop team. Therefore, the initial HIRENASD structural model has been first of all improved within AePW, and provided to the AePW community, together with the experimental data.

3 NUMERICAL SOFTWARES

3.1 elsA

The compressible 3-D Reynolds-averaged Navier-Stokes equations for arbitrary moving bodies are solved on multi-block structured meshes by a cell centered finite-volume method with central space discretization. The discrete equations are integrated by backward Euler integration with implicit LU schemes. For time accurate computations, the implicit dual time stepping method is employed. A large variety of turbulence models is available, but only the Spalart-Allmaras one-equation model and the K-ω two-equation model of Kok are used here.

The approach implemented in elsA/Ael for static coupling simulations is based on a "reduced flexibility matrix", which is derived from the NASTRAN finite element model. This approach assumes that the structure is linear. Two sets of structural nodes are selected in the finite element model: a set of "force" nodes $\{X_f\}$, on which the aerodynamic loads will be transferred, and a set of "displacement" nodes $\{X_d\}$, which will be used to transfer the

structural deformations on the aerodynamic surface grid. The reduced flexibility matrix is then generated in a pre-processing step, performing a NASTRAN static computation with several subcases. In each subcase computation, a unit load is applied to one "force" node, and each subcase computation provides one column of the reduced flexibility matrix, *S*. For a linear structural model, the displacements *D* on $\{X_d\}$ are then connected to the forces *F* applied on $\{X_f\}$ by:

$$D = S\,F \tag{1}$$

The following steps are achieved at each coupling cycle, until convergence of the fluid-structure coupling process:

- Computation of the flow solution over N time-steps, using the local time-stepping technique.
- Computation of the loads on the aerodynamic surface grid.
- Transfer of loads on the structural grid (computation of *F* in (1)).
- Computation of the displacements *D* on the structural grid using the flexibility matrix.
- Transfer of the displacements on the aerodynamic surface grid.
- Deformation of the aerodynamic grid.

When large displacements are encountered, an under-relaxation coefficient is applied in order to stabilize the coupling iteration. Transfers of loads and displacements between the aerodynamic and structural grids are then performed component-wise, with the necessity to ensure the continuity of the displacements between the different components. In step 2, the aerodynamic forces are computed at the center of each wall cell interface. These forces are transformed in step 3 into an equivalent force-moment system operating on the set of "force" structural nodes. To achieve this, each structural "force" node and fluid wall cell interface are associated using a "closest neighbor" type strategy. The deflections computed on the structural nodes are transferred back to the aerodynamic grid using global interpolation techniques, such as the infinite plate technique, or fitting techniques, such as polynomial fitting in 1D or 2D. In the present simulations, the mesh deformation technique, used to propagate the structural displacements in the surrounding aerodynamic grid, is based on a mixed analytical/transfinite interpolation technique.

Non-linear forced motion simulations may also be performed. In the case of a prescribed structural mode harmonic motion, the computation is run over several periods of motion in order to get a periodic aerodynamic response. The aerodynamic temporal response of the fluid gives access to unsteady pressure distributions on the model surface.

3.2 EZNSS

The EZNSS code is a multi-zone Euler/ Navier-Stokes flow solver which is capable of simulating complex, time-accurate flows about dynamically deforming geometries. The diffusive fluxes of the mean flow equations and of the turbulence model equation are discretized using second-order central differencing based on a full-viscous stencil. The convective flux vector of the mean-flow equations may be approximated by second-order central differencing via the Beam & Warming algorithm or by upwind schemes such as the flux vector splitting by Steger-Warming or by an approximate Riemann solver such as the HLLC [9] and the AUSM+-up scheme [10]. The left and right states of the approximate Riemann solvers are evaluated using a third-order biased MUSCL scheme. The convective

flux of the turbulence model is approximated by the HLLC scheme based on the passive scalar approach using a third-order biased MUSCL scheme. The code provides the choice between various implicit time marching schemes for the mean-flow equations, such as the AF-ADI method, the DDADI method [11], and the line Gauss-Seidel method. The time marching scheme that is used for the turbulence models is the unconditionally positive-stable scheme developed by Mor-Yossef and Levy [12,13]. Second order temporal accuracy is achieved by using dual-time stepping computational surface mesh.

ENZSS solves the static or dynamic aeroelastic equation of motion (EOM) in modal coordinates. The generalized mass and stiffness matrices and the modes matrix are generated by a finite-element code and provided as inputs to the aeroelastic simulation. A spline routine, based on the Infinite Plate Spline (IPS) [14] and beam spline algorithms, is used to map the modes from the finite-element nodes in which they are computed to the CFD surface mesh.

In the dynamic aeroelastic case, the aeroelastic EOM is solved for the generalized displacements following each CFD iteration. In the static case, the static aeroelastic EOM is solved following a user-defined number of CFD iterations, typically in the order of 100. This leads to an efficient aeroelastic scheme in which the elastic shape and the flow solution converge concurrently, while applying only a small number of elastic shape updates. The block-diagram describing the elastic solution procedure is presented in [15]. Following each solution of the static aeroelastic EOM, the generalized deformations are used to compute the displacements at the computational surface grids, which are then mapped to the whole volume grid using a shearing method [15].

4 COMPUTATIONAL RESULTS

Static coupling for the prediction of steady state flow and dynamic response to a prescribed excitation have been carried out by the partners and compared with the available experimental data.

4.1 The CFD meshes

ONERA has used two structured multi-block CFD grid. The first grid has been generated by Thorsten Hanssen, Ansys Germany, following the gridding guidelines defined in the AePW workshop. With a total of about 6.5 millions grid points, this structured mesh corresponds to the AePW definition of a coarse grid (Figure 2). The second one has been generated by Airbus France. With a total number of nodes of about 30 millions grid points, this mesh corresponds to the AePW definition of a fine grid (Figure 3). In these meshes, the farfield is located at about 100 c_{ref} (c_{ref} being the reference chord length of the wing) and the initial spacing normal to all walls should correspond to y^+ ~1 for the coarse grid and 4/9 for the fine grid.

Figure 4 displays the structural nodes that have been selected on the wing, in order to build the reduced flexibility matrix used in elsA/Ael for the static coupling simulations.

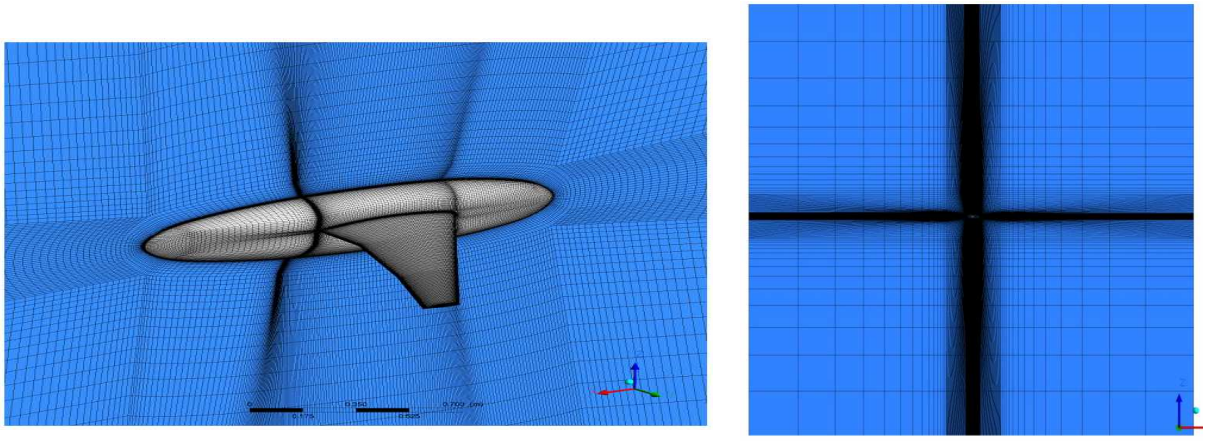

Figure 2: Partial view of the coarse grid

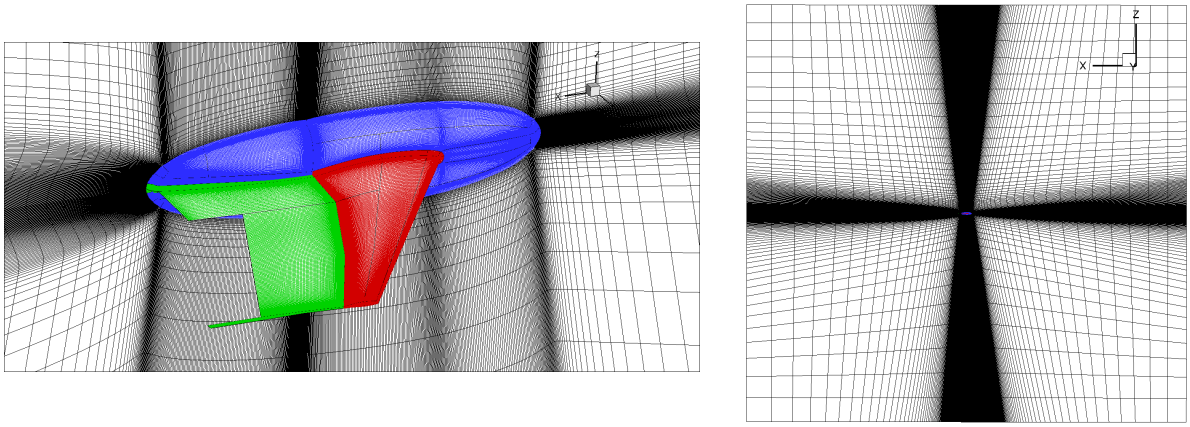

Figure 3: Partial view of the fine grid

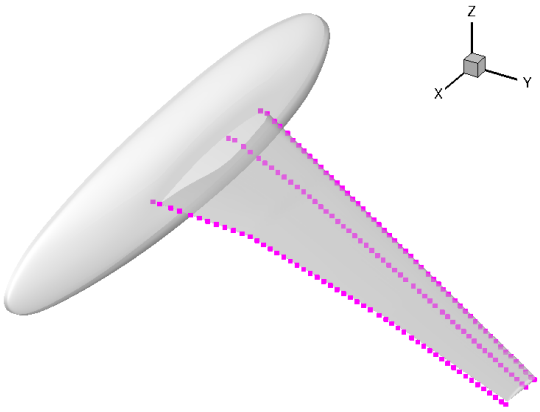

Figure 4: skin model structural nodes

The structure computation and update of the aerodynamic grid are achieved every 100 CFD iterations. Convergence has been accelerated using the multigrid technique, only for the fine grid.

The computational mesh for the HIRENASD configuration, with the EZNSS code, has grid zones for the wing, fuselage, a "world" zone, and a collar zone for matching flow conditions between the fuselage and wing zones (Figure 5). With a total of about twelve million grid

points this mesh corresponds to the AePW definition of a medium mesh. Flow simulations were conducted using the HLLC scheme and the Spalart-Allmaras with Edwards and Chandra's modifications turbulence model.

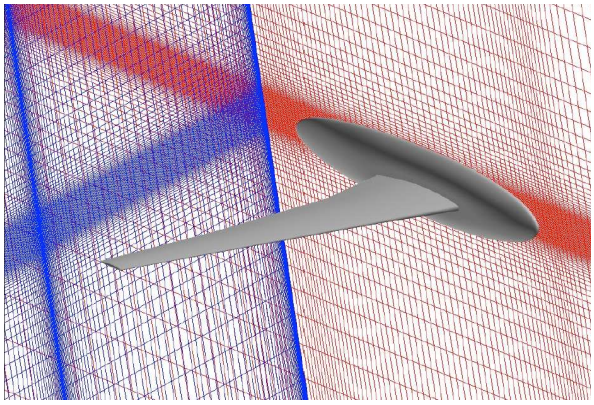

(a) World

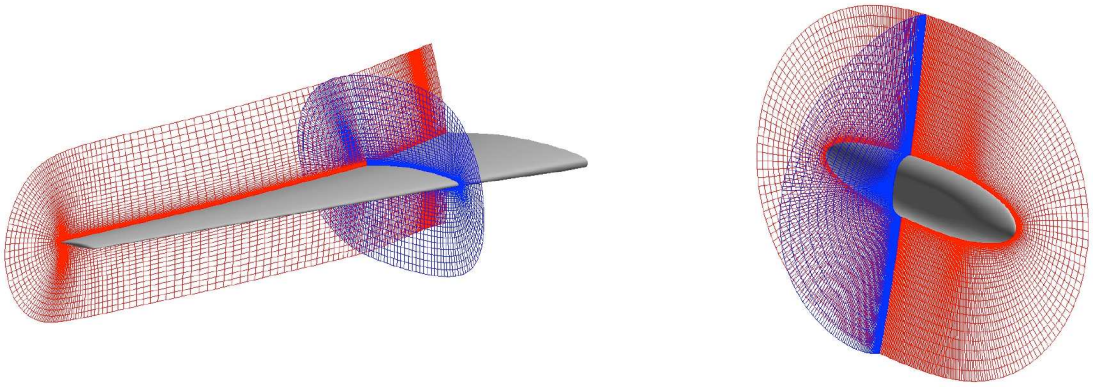

(b) Wing (c) Fuselage

Figure 5: HIRENASD computational mesh

Static modal aeroelastic analysis is based on thirty modes of the wing only. The mode shapes, computed by MSC/Nastran modal analysis, were provided at 176 nodes along the wing, and mapped to the computational surface mesh, as part of the EZNSS analysis, based on the Infinite Plate Spline method. Figure 6 presents the first two modes, on the computational surface mesh.

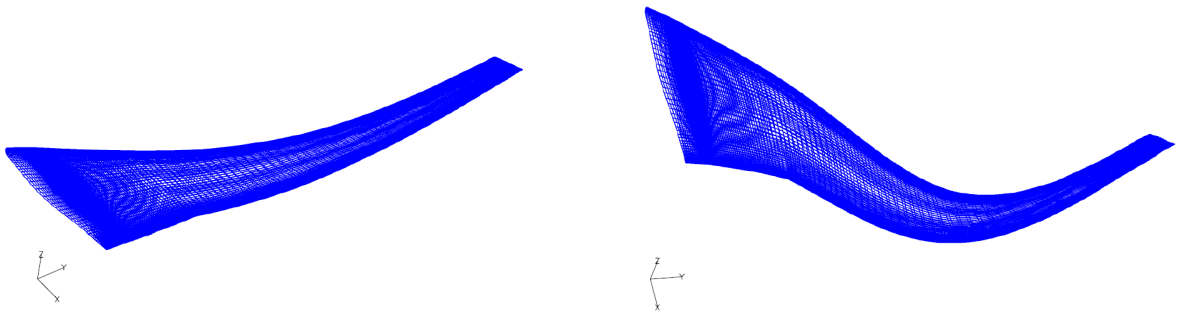

(a) Mode 1 (b) Mode 2

Figure 6: HIRENASD first two elastic modes, mapped to computational grid

4.2 Results of steady aeroelastic simulations

Figures 7, 8 and 9 present the pressure coefficients (Cp) in the experimental sections, and compare the elsA/Ael results on the coarse (C) and fine (F) grids, and the EZNSS results on the medium (M) grid, , with the experimental data.

At Mach number 0.7 and Reynolds number 7 million, all computed Cp are in good agreement with the experimental data. At Mach number 0.8 and Reynolds number 7 million, a small difference confined to the upper surface shock location appears between the different solutions. A larger deviation can be observed at Reynolds number 23.5 million in the first section close to the wing root, between the simulations and the experimental data. The experimental and computational results are however very close in the other sections for this high Reynolds number case.

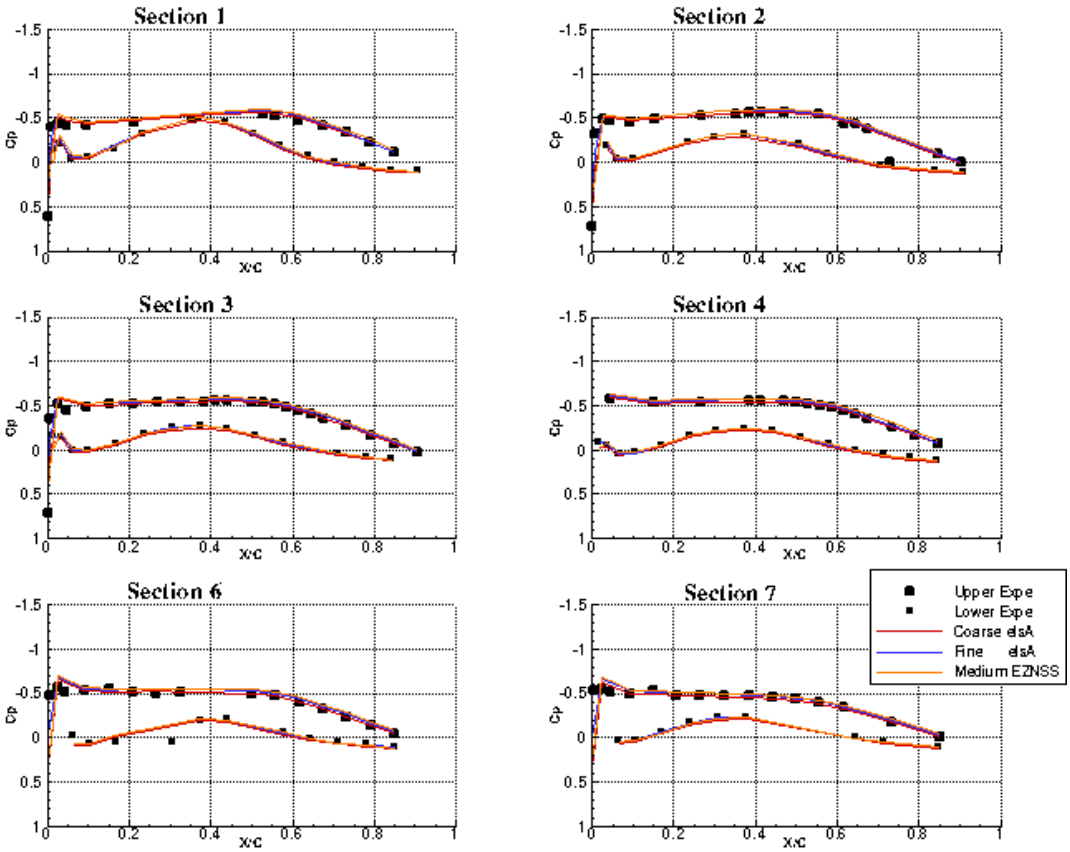

Figure 7 : Static coupling simulations for test case no 155; Mach=0.7, $Re_c=7*10^6$, α=1.5°. Comparison for coarse/fine grid (elsA) and mid grid (EZNSS)

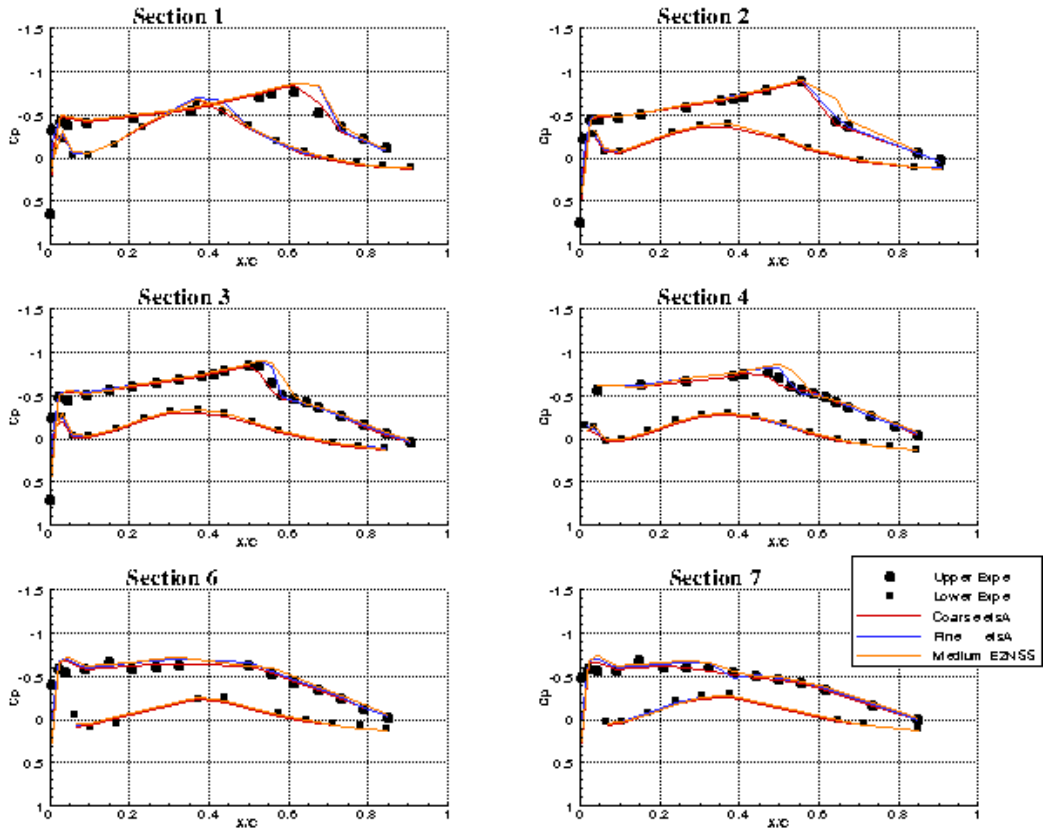

Figure 8 : Static coupling simulations for test case no 159; Mach=0.8, $Re_c=7*10^6$, α=1.5°. Comparison for coarse/fine grid (elsA) and mid grid (EZNSS)

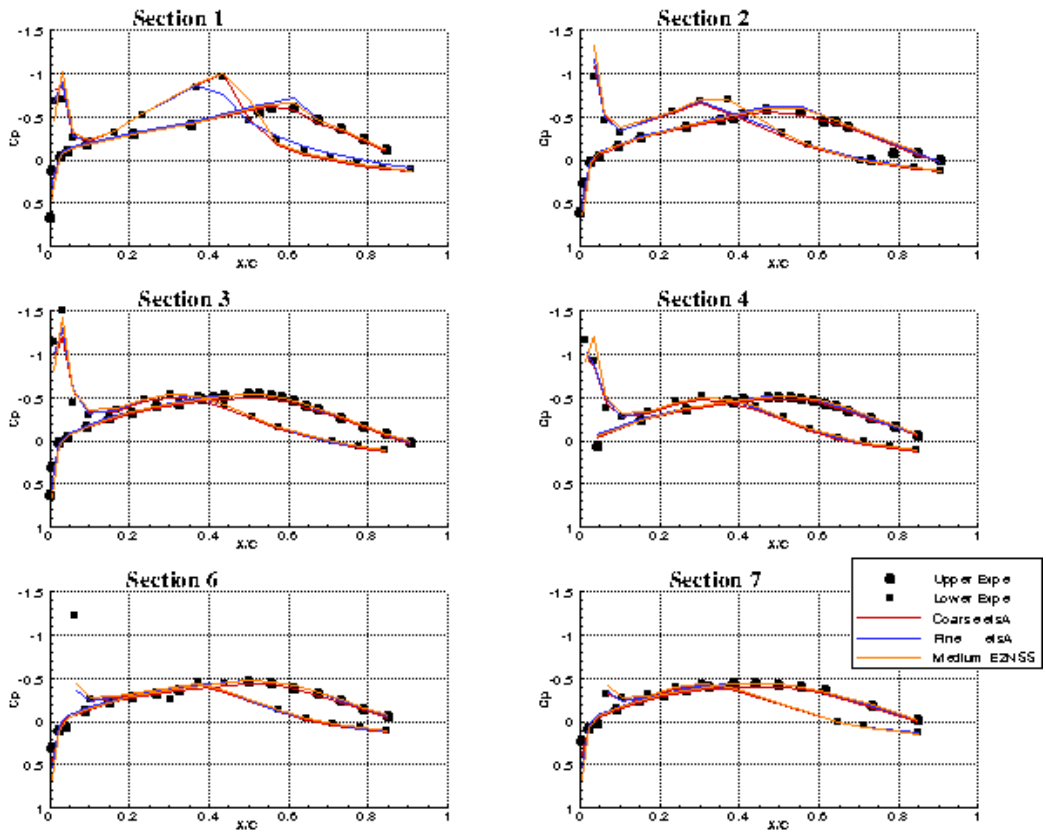

Figure 9 : Static coupling simulations for test case no 271; Mach=0.8, $Re_c=23*10^6$, α=-1.34°. Comparison for coarse/fine grid (elsA) and mid grid (EZNSS)

Figure 10 illustrates the steady state convergence histories using elsA/Ael for test case no 159. A good convergence level of the flow residual (density) is obtained after 3000 iterations in the fine grid with multi-grid techniques and after 4000 iterations in the coarse grid without convergence acceleration. The integrated aerodynamic coefficients predicted by the elsA coarse grid and fine grid simulations are very similar for this low Reynolds number case.

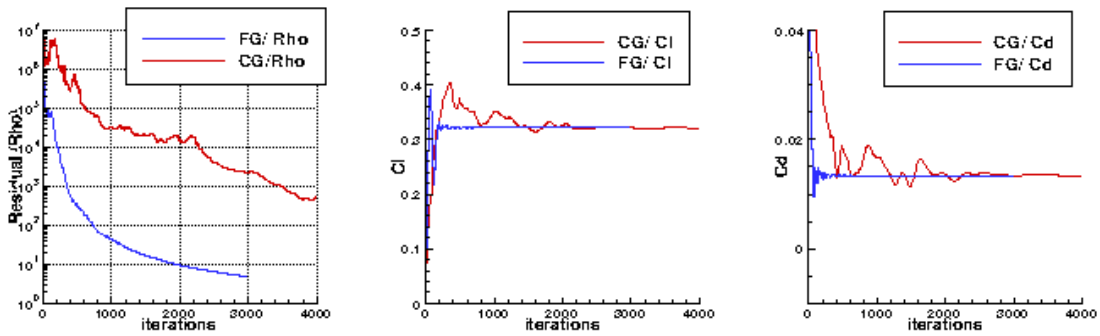

Figure 10 : Steady State convergence histories for test case no 159; Mach=0.8, $Re_c=7*10^6$, $\alpha=1.5°$. Comparison for coarse/fine grid, elsA computations

The global aerodynamic coefficients obtained from the different static aeroelastic calculations are shown in table 1. At Reynolds number 7 million, these coefficients are very close. The difference is larger at Reynolds number 23.5 million, but for this case, the solution on the fine grid did not converge as well as the medium and coarse grid computations.

Case 155	C_L	C_D	C_M
Coarse mesh	0.2893	0.0117	-0.2322
Medium grid	0.2924	0.0106	-0.4624
Fine Mesh	0.2907	0.0112	-0.2335

Case 159	C_L	C_D	C_M
Coarse mesh	0.3201	0.0134	-0.2619
Medium grid	0.3334	0.0130	-0.5221
Fine Mesh	0.3223	0.0134	-0.2653

Case 271	C_L	C_D	C_M
Coarse mesh	0.0158	0.00963	-0.0817
Medium grid	-0.0172	0.009	-0.0975
Fine Mesh	0.0259	0.01103	-0.0813

Table 1 : Computed Aerodynamic Coefficients.

The spanwise bending and twist deformations are displayed in Figure 11 for the elsA coarse grid and EZNSS medium grid computations. It appears that for the three test cases, the vertical deflections predicted by elsA/Ael are slightly lower than those computed by EZNSS. However the twist distributions are very similar.

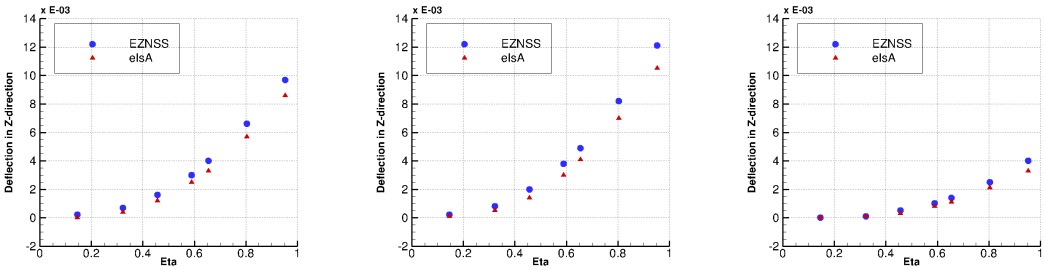

Figure 11a : Bending for Test case no 155,159, 271. Comparison for coarse/medium grid

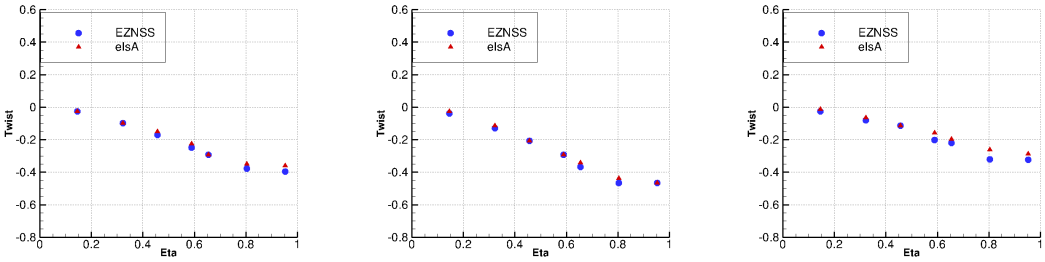

Figure 11b : Twist for Test case no 155,159, 271. Comparison for coarse/medium grid

ONERA has investigated the influence of turbulence modelling on the numerical results. Two different turbulence models, the 1-equation Spalart-Allmaras and the 2-equation K-ω model, were used in the coarse grid coupled simulations with elsA/Ael.

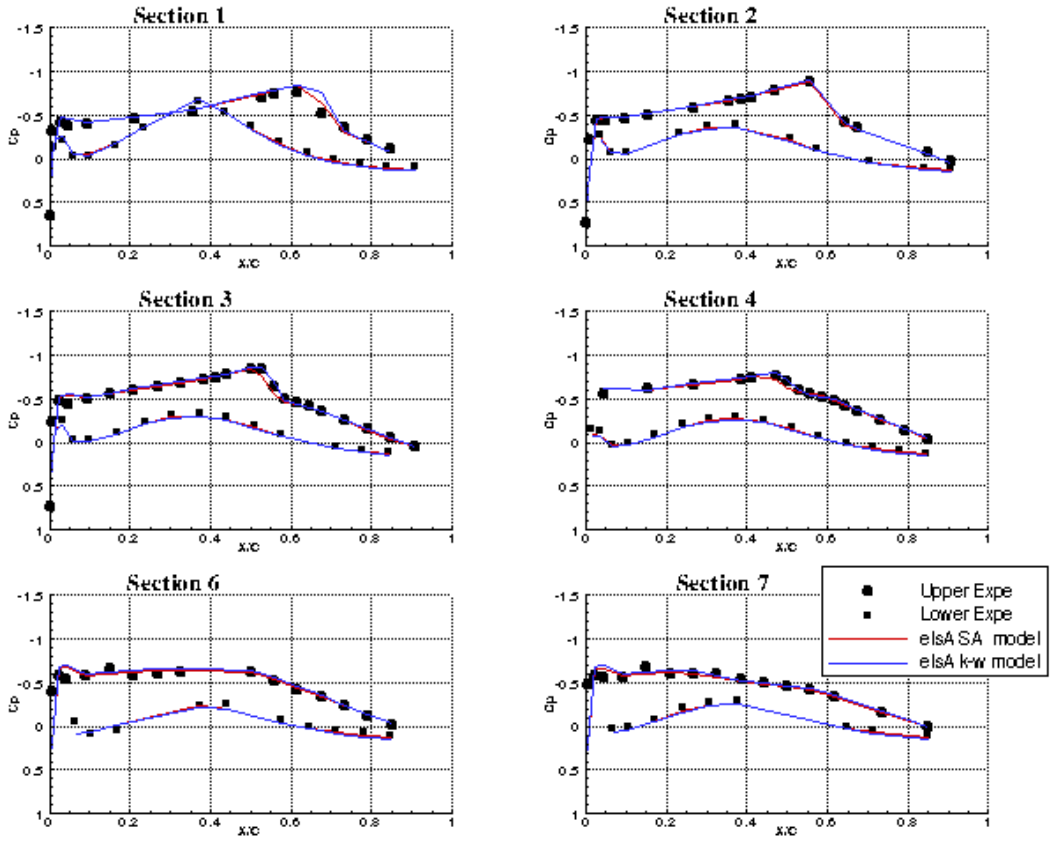

Figure 12 : Static coupling simulations with elsA for Test case no 159; Mach=0.8, $Re_c=7*10^6$, α=1.5°. Influence of turbulence modelling (SA versus K-ω)

It was observed that the change of turbulence model has only a very minor impact on the solution, both for the low and high Reynolds number cases. An example of comparison between the 2 solutions is presented in Figure 12, for Data Point 159 (Reynolds number 7 million and Mach number 0.8).

4.3 Results of the unsteady aeroelastic simulation

The forced motion for the Hirenasd configuration was generated by exciting the wing second bending mode near its natural structural frequency. For test case no 159, the frequency of oscillation is f=78.9Hz and the reference amplitude of excitation is Δz=2.4mm. Figure 13 and Figure 14 show the Fourier analysis of the pressure coefficient (magnitude and phase part of 1st harmonic) in six experimental sections. The results were post processed to produce the frequency response function (FRF) of the pressure due to displacement at accelerometer 15. The displacement value was normalized by the reference chord. Unsteady elsA/Ael simulations were performed for both grids, using 64 physical steps per oscillation period. The unsteady solutions were started from the static aeroelastic solutions, and 4 cycles were sufficient in order to get a well converged periodic solution. The dual time stepping technique has been used for all unsteady computations. Convergence of the dual time-stepping loop is based on the ρ residual, with however a limit value for the total number of dual iterations per physical time step equal to 50. The simulated pressure coefficients using EZNSS are also shown. In this case, time-accurate aerodynamic response to the prescribed modal excitations at the provided flow conditions was performed using a physical time step of 5E-5 seconds (which corresponds to approximately 250 iterations per cycle), with additional 10 flow sub-iterations in between two consecutives time steps.

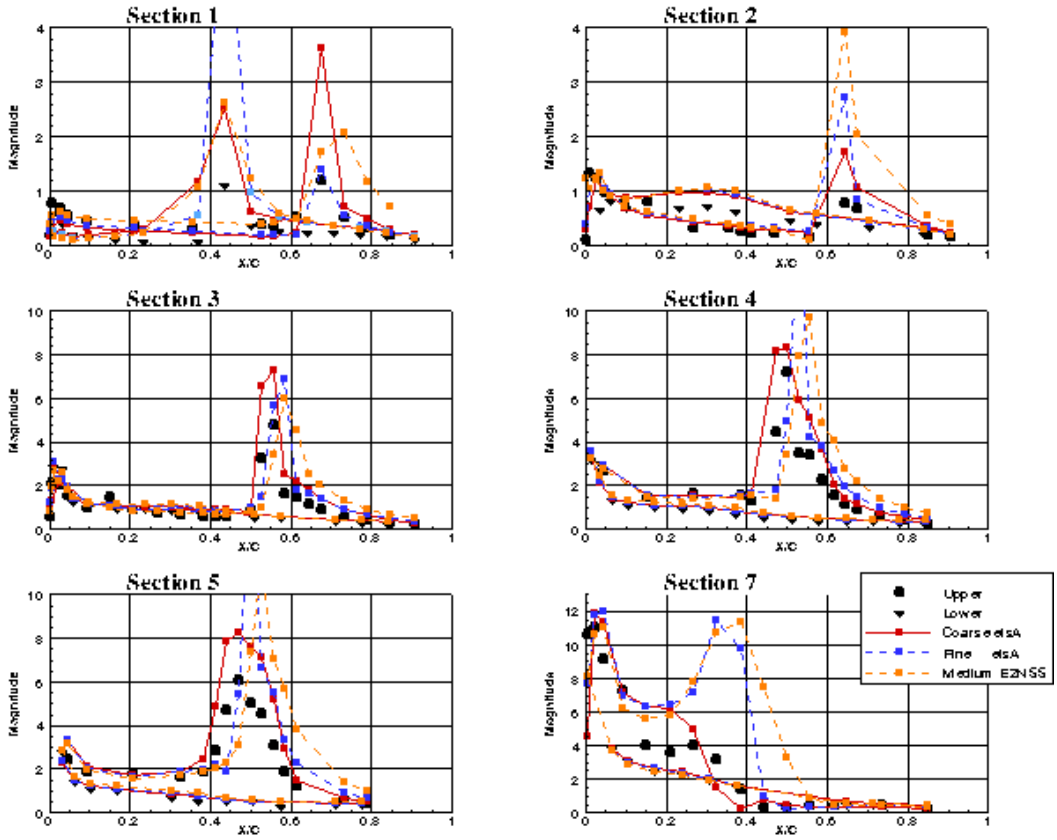

Figure 13 : Magnitude of the unsteady pressure coefficient for test case no 159; Mach=0.8, $Re_c=7*10^6$, α=1.5°. Comparison between elsA/Ael coarse/fine grid and EZNSS medium grid solutions

Near the leading edge, the simulation matches the magnitude reasonably. In the shock region on the upper surface, the peak of the simulation is well positioned. The level of the peak is stronger in the case of the fine grid. The computed shock is located at a rear position with respect to the experimental data. The lower surface pressures are well predicted.

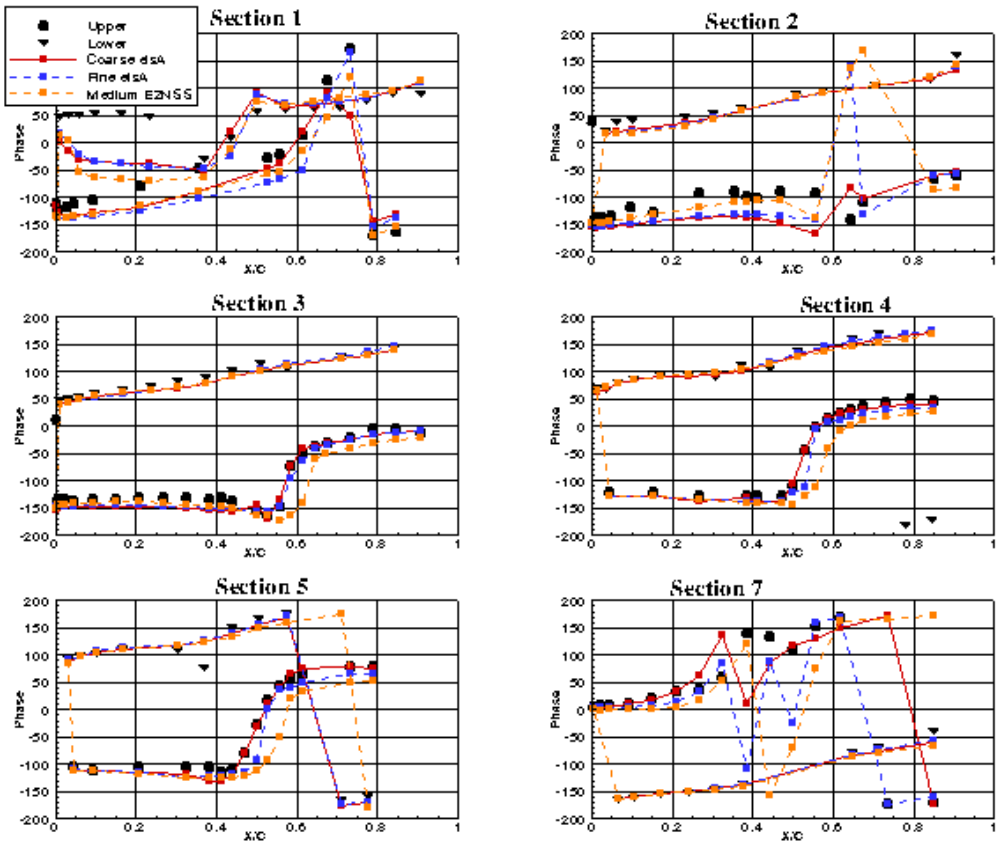

Figure 14 : Phase of the unsteady pressure coefficient for test case no 159; Mach=0.8, $Re_c=7*10^6$, α=1.5°. Comparison between elsA/Ael coarse/fine grid and EZNSS medium grid solutions

ONERA has also investigated the influence of time discretization and convergence level. This has been achieved only using the coarse grid, for test case 159. Three unsteady simulations have been compared, with 2 different physical time step sizes, and 2 different maximum numbers of inner iterations, see below. The maximum number of dual-time iterations is reached at each physical time step in run 1 and run 3, whereas convergence of the inner loop is obtained in run 2 in about 70 iterations. Figure 15 and Figure 16, presenting respectively the modulus and phase of the unsteady pressures, show that quasi identical solutions are predicted by the three computations, with only some very small deviations in section 5 on the pressure levels near chock.

Run	Number of time steps per period (physical time loop)	Maximum number of inner iterations (dual time loop)
1	64	50
2	64	100
3	32	100

Table 2 : Numerical parameters investigated for time discretization and convergence level

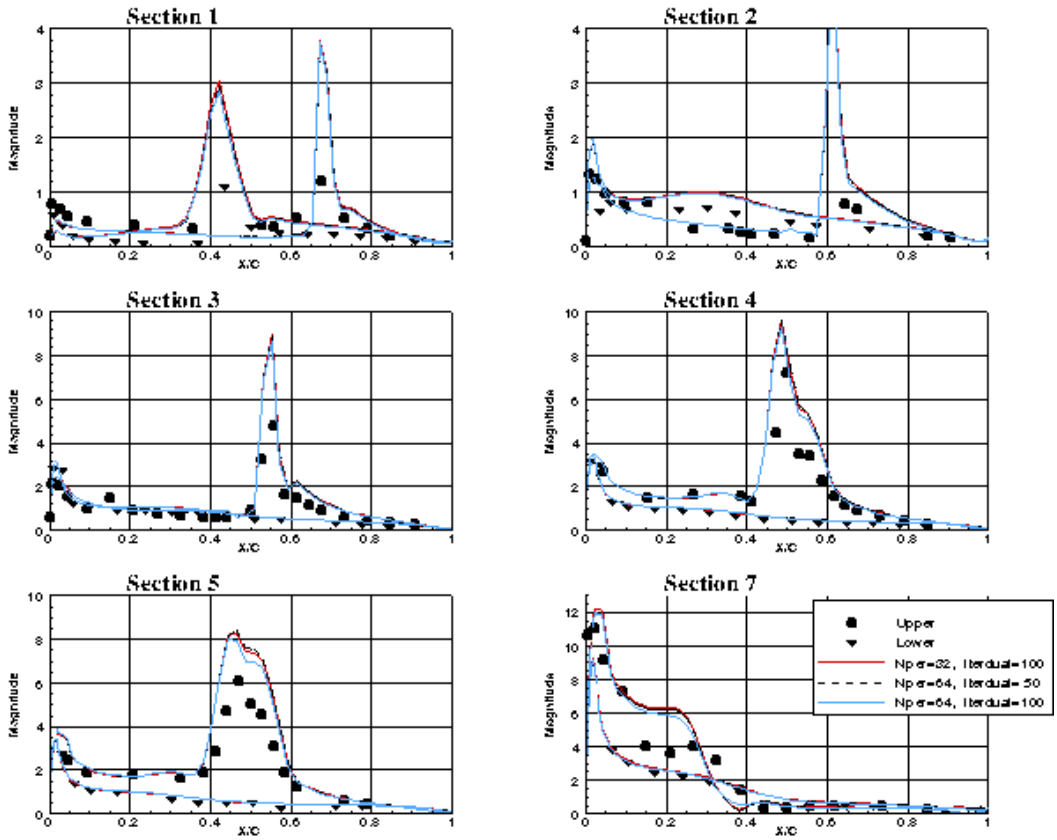

Figure 15 : Magnitude of the unsteady pressure coefficient for test case no 159; Mach=0.8, $Re_c=7*10^6$, α=1.5°.

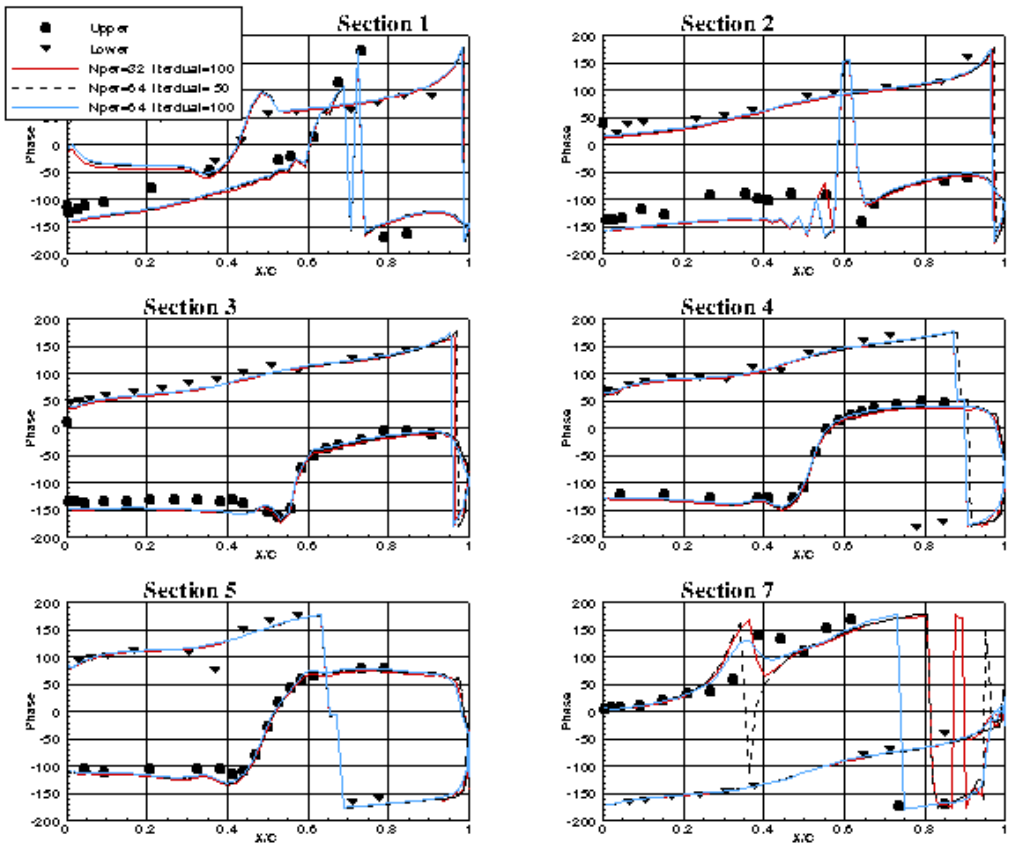

Figure 16 : Phase of the unsteady pressure coefficient for test case no 159; Mach=0.8, $Re_c=7*10^6$, α=1.5°.

5 CONCLUSIONS

Aeroelastic RANS and URANS simulations, using two different structured softwares, EZNSS and elsA/Ael, were performed in the case of the HIRENASD configuration for the first aeroelastic workshop (AePW). A good agreement was observed between the static coupling numerical simulations and the experimental data, for all the investigated cases. Small deviations appear however at the shock location, depending on the grid used. The flow solutions based on the k-ω model and the one equation model of Spalart-Allmaras are nearly identical. Time-accurate aerodynamic responses to a prescribed modal excitation have been performed at M=0.8 and Re_c=7 million. A general good agreement is observed on the unsteady pressure levels between the different simulations and the experimental results, with however larger deviations at the wing tip, and an overestimation of the peak values in the shock region.

6 REFERENCES

[1] Heeg J. et al., "Overview of the Aeroelastic Prediction Workshop", AIAA paper 2013-0783, Grapevine, TX, January 2013.

[2] Ballmann J et al.,"The HIRENASD project: High Reynolds Number Aerostructural Dynamics Experiments in the European transonic Windtunnel(ETW)", ICAS Paper 2006-726, September 2006.

[3] Ballmann J. et al.," Experimental Analysis of High Reynolds Number Aerostrutural Dynamics in ETW", AIAA Paper 2008-841, Reno, Nevada, January 2008.

[4] Reimer L. et al., "Computational Aeroelastic Design and Analysis of the HIRENASD Wind Tunnel Wing Model and Test", IFASD 2007

[5] Cambier, L., and Gazaix, M., "elsA: An Efficient Object-Oriented Solution to CFD Complexity", 40th AIAA Aerospace Sciences Meeting and Exhibit, 14-17 January 2002, Reno, Nevada, AIAA-2002-0108.

[6] Cambier, L., Heib, S., Plot, S., The ONERA elsA CFD software: Input from Research and Feedback from Industry, ICAS 2012, 23 - 28 September, 2012, Brisbane, Australia

[7] Girodroux-Lavigne, P., "Progress in steady/unsteady fluid-structure coupling with Navier-Stokes equations", International Forum on Aeroelasticity and Structural Dynamics, 28 June – 1 July 2005, Munich, Germany.

[8] Dugeai, A., "Aeroelastic Developments in the *elsA* Code and Unsteady RANS Applications", International Forum on Aeroelasticity and Structural Dynamics, 28 June – 1 July 2005, Munich, Germany.

[9] P. Batten, M. A. Leschziner, and U. C. Goldberg. Average-state Jacobians and implicit methods for compressible viscous and turbulent flows. Journal of Computational Physics, 137(1):38–78, 1997.

[10] Meng-Sing Liou. A sequel to AUSM, part II:AUSM+-up for all speeds. Journal of Computational Physics, 214(1):137–170, 2006.

[11] G. H. Klopfer, R. F. Van der. Wijngaart, C. M. Hung, and J. T. Onufer. A diagonalized diagonal dominant alternating direction implicit (D3ADI) scheme and subiteration correction. In 29th Fluid Dynamics Conference, Albuquerque, NM, June 1998. AIAA paper 1998 - 2824.

[12] Y. Mor-Yossef and Y. Levy. The unconditionally positive-convergent implicit time integration scheme for two-equation turbulence models: Revisited. Computers & Fluids, 38(10):1984–1994, 2009.

[13] Y. Mor-Yossef and Y. Levy. Desiging a positive second-order implicit time integration procedure for unsteady turbulent flows. Computer Methods in Applied Mechanics and Engineering, 196(41-44):4196–4206, 2007.

[14] Harder R. L. and Desmarais R. N. Interpolation Using Surface Splines. Journal of Aircraft, 9(2):189–191, 1972.

[15] Raveh D. E., Levy Y., and Karpel M. Structural Optimization Using Computational Aerodynamics. Journal of Aircraft, 38(10):1974–1982, 2000.